College of Engineering

ISSN: 1813-162X (Print) ; 2312-7589 (Online)

Tikrit Journal of Engineering Sciences

available online at: http://www.tj-es.com

TJES
Tikrit Journal of Engineering Sciences

Hybrid CFD-ANN Scheme for Air Flow and Heat Transfer Across In-Line Flat Tubes Array

Ataalah Hussain Jassim [1]

M.M. Rahman [2]

Khalaf Ibrahim Hamada [1]

M. Ishak [2]

Tahseen Ahmad Tahseen [1,*]

[1] Department of Mechanical Engineering
College of Engineering
Tikrit University
Tikrit, Iraq

[2] Faculty of Mechanical Engineering
Universiti Malaysia Pahang
26600 Pekan
Pahang, Malaysia

***Keywords*:**

In-line flat tube
finite volume technique
CFD
modeling
friction factor
artificial neural networks

ARTICLE INFO

Article history:

Received	14 November 2017
Accepted	06 March 2018
Available online	17 June 2018

ABSTRACT

Flat tubes are vital components of various technical applications including modern heat exchangers, thermal power plants, and automotive radiators. This paper presents the hybridization of computational fluid dynamic (CFD) and artificial neural network (ANN) approach to predict the thermal-hydraulic characteristics of in-line flat tubes heat exchangers. A 2D steady state and an incompressible laminar flow in a tube configuration are considered for numerical analysis. Finite volume technique and body-fitted coordinate system are used to solve the Navier–Stokes and energy equations. The Reynolds number based on outer hydraulic diameter varies between 10 and 320. Heat transfer coefficient and friction are analyzed for various tube configurations including transverse and longitudinal pitches. The numerical results from CFD analysis are used in the training and testing of the ANN for predicting thermal characteristics and friction factors. The predicted results revealed a satisfactory performance, with the mean relative error ranging from 0.39% to 5.57%, the root-mean-square error ranging from 0.00367 to 0.219, and the correlation coefficient (R^2) ranging from 99.505% to 99.947%. Thus, this study verifies the effectiveness of using ANN in predicting the performance of thermal-hydraulic systems in engineering applications such as heat transfer modeling and fluid flow in tube bank heat exchangers.

DOI: http://dx.doi.org/10.25130/tjes.25.2.08

نظام ديناميكا الموائع الحسابية والشبكة العصبية الاصطناعية الهجين لانتقال الحرارة وجريان الهواء عبر حزمة انابيب مسطحة مرتبة بشكل خطي

الخلاصة

الأنابيب المسطحة هي المكونات الحيوية لمختلف التطبيقات التقنية بما في ذلك المبادلات الحرارية الحديثة، ومحطات الطاقة الحرارية، ومشعات السيارات. يعرض هذا البحث استخدم عملية التهجين لديناميك الموائع الحسابية (CFD) والشبكة العصبية الاصطناعية (ANN) للتنبؤ بالخصائص الحرارية والهيدروليكية للمبادلات الحرارية ذات الانابيب المسطحة. اعتبرت حالة الجريان مستقرة وببعدين وطباقي التدفق وغير قابل للانضغاط في التحليل العددي. استخدمت تقنية الحجم المحـدود (finite volume technique) ونظام تطابق الاحداثيات (body-fitted coordinate) لحل معادلات نافير- ستوك (Navier–Stokes) ومعادلة الطاقة. حسب عدد رينولدز على أساس القطر الهيدروليكي الخارجي للأنبوب وبمدى 10 الى 320. تم تحليل معامل انتقال الحرارة والاحتكاك لجميع الحالات المدروسة للمسافة بين مركز الانابيب العرضية والطولية. استخدمت النتائج العددية من تحليل الـ (CFD) في تدريب واختبار الشبكة العصبية الاصطناعية للتنبؤ بالخصائص الحرارية وعامل الاحتكاك. أظهرت النتائج المتوقعة من الشبكة العصبية الاصطناعية أداء مرضيا، حيث تراوح متوسط الخطأ النسبي بين 0.39٪ و5.57٪، وكان مدى مربع متوسط جذر الخطأ من 0.00367 إلى 0.219، وتراوح معامل الارتباط (R^2) من 99.505٪ إلى 99.947٪. وبالتالي، فإن هذه الدراسة تتحقق من فعالية استخدام الشبكة العصبية الاصطناعية في التنبؤ في أداء المنظومات الحرارية والهيدروليكية وكذلك في التطبيقات الهندسية المختلفة مثل نمذجة انتقال الحرارة وتدفق الموائع في المبادلات الحرارية ذات حزم الانابيب.

1. INTRODUCTION

The fluid flow and heat transfer in tube banks demonstrate the real-life applications of various industrially significant processes. Tube bundles are widely employed in cross-flow heat exchangers, and their design is based on the empirical correlations of heat transfer and pressure drop. Cross-flow heat exchangers with tube banks are essential to numerous thermal and chemical engineering processes [1–4]. Flat tube designs have been recently introduced for modern heat exchanger applications such as automotive radiators. Unlike circular

* *Corresponding author: E-mail* : tahseen@tu.edu.iq ; tahseen444@gmail.com

Nomenclature

c_P	specific heat capacity of fluid, (J/kg K)
D_h	hydraulic diameter of tube, (m)
d_L	longitudinal diameter of tube, (m)
d_T	transverse diameter of tube, (m)
G_1^*, G_2^*	contravariant velocity components
J^*	Jacobian of the transformation
k	thermal conductivity of fluid, (W/m K)
N_L	number of rows in flow direction
p	pressure, (Pa)
P_1	longitudinal distance, (m)
P_2	transverse distance, (m)
P_L	longitudinal pitch
P_T	transverse pitch
S	source term
T	temperature, (°C)
u, v	velocity components, (m/s)
U_1, U_2	dimensionless velocity
x, y	Cartesian coordinates, (m)

Dimensionless groups

f	friction factor
j	Colburn factor
Nu	overall Nusselt number
Re	Reynolds number

Greek symbols

μ	dynamic viscosity, (kg/m s^2)
ρ	density, (kg/m^3)
α, β, γ	coefficients of transformation

Subscripts

*	dimensionless quantity
N	numerical data
out	outlet
w	tube wall

tubes, flat tubes have appropriate pressure drop characteristics [5-7].

Artificial neural networks (ANN) are used in numerous engineering applications because these tools provide excellent and highly reasonable solutions [8]. Ermis et al. [9] used a feed-forward back-propagation ANN to conduct numerical and experimental analysis of the heat transfer resulting from the phase change process in finned tubes. The experimental study yielded a mean relative error of 5.58%, whereas that of the numerical model is 14.99%. Fadare and Fatona [10] studied ANN in modeli-ing staggered multi-row, multi-column in cross-flow, tube-to-tube heat exchangers, as well as the experimental data for air flow over a bundle of tubes. Results demonstrated that the mean absolute relative errors are less than 4% and 1% for the testing and training data sets, respectively. Islamoglu and Kurt [11] used an ANN to model the predicted heat transfer in corrugated channels. The mean absolute error between the experimental results and the ANN approach was less than 4%. The developed ANN models for predicting heat transfer coefficient and friction factor in helically coiled tubes used the empirical data for the prediction, which is then compared with previously published experimental correlations [12,13].

This study focuses on the applicability of ANN for the analyses of heat transfer and friction factor in in-line flat tube banks. Such analyses elucidate whether the use of in-line flat tube banks in the design of heat exchangers promotes heat transfer. CFD simulation results are compared with ANN model results, and various geometrical parameters on heat transfer coefficient and friction factor are discussed.

2. CFD SIMULATION AND FORMULATION

Four horizontal flat tubes isothermal heated in the row at the direction of the external flow. A flat tube with two outside diameters, namely, transverse d_T and longitudinal d_L, as well as the surface temperature of tube T_s placed in the velocity u_∞ and the uniform inlet free stream of temperature T_∞ in the in-line arrangement are used. The three longitudinal pitch-to-outside small diameter (transverse) ratio, $P_L = P_1/d_T$, are 3.0, 4.0, and 6.0, and the four transverse pitch-to-outside small diameter ratio, $P_T = P_2/d_T$, are 1.5, 2.5, 3.5, and 4.5. A sufficiently long flat tube is required to neglect the end effect of the tube. Therefore, flow field is assumed to be two-dimensional. The tube configuration and flow field calculation for the in-line flat tube banks are presented in Fig. 1(a).

The governing equations are transformed into dimensionless forms upon incorporating the following non-dimensional variables.

$$\left.\begin{aligned} &(x^*, y^*) = \frac{(x,y)}{D_h}, \quad p^* = \frac{p}{\rho \times (u_\infty)^2}, \\ &(U_1, U_2) = \frac{(u,v)}{u_\infty}, \quad T^* = \frac{T - T_\infty}{T_s - T_\infty}, \\ &Re_{D_h} = \frac{u_\infty \times D_h}{\upsilon}, \qquad Pr = \frac{\mu \times c_P}{k} \end{aligned}\right\} \tag{1}$$

The outer side hydraulic diameter of the flat tube can be written as follows:

$$D_h = \frac{4 \times \left[\frac{\pi}{4} d_T^2 + (d_L - d_T) \times d_T\right]}{\pi d_T + 2(d_L - d_T)} \tag{2}$$

where (x, y) are the Cartesian coordinates, m; ρ is the air density, kg/m^3; p is pressure, N/m^2; u_{in} is the air inlet velocity, m/s; (u, v) is the velocity components of fluid, m/s; T is the fluid temperature, °C; T_{in} is the inlet free stream temperature, °C; T_w is the surface temperature of tube, °C; D_h is the outside hydraulic diameter of the tube, m; d_L is the outside longitudinal diameter of tubes, m; d_T is the outside transverse diameter, m; μ is the air dynamic viscosity, kg/(m s); c_P is the air specific heat, J/(kg K); and k is the air thermal conductivity, W/(m K).

The following assumptions are made in developing the model: (i) the physical properties of air flow are constant; (ii) the air flow is incompressible and laminar flow; and (iii) steady-state flow and heat transfer. The governing equations for 2D continuity and Navier–Stokes for momentum and energy can be written as follows [14]:

The continuity equation

$$\nabla . \mathrm{v} = 0 \tag{3}$$

Momentum (Navier-Stokes) equation

$$\rho \nabla(\mathrm{vv}) = -\nabla P + \mu \nabla . (\nabla \mathrm{v}) \tag{4}$$

Energy equation

$$\nabla(\mathrm{vT}) = \frac{k}{\rho\, c_P}\nabla.(\nabla\mathrm{T}) \tag{5}$$

In Eqs. (3) and (4), v is the velocity vector (u, v).

The physical system considered in this study is illustrated in Fig. 1(a). The boundary conditions used for the solution domain are uniform inlet velocity, fully developed outflow, and combined symmetry and no-slip tube surfaces at the bottom and top boundaries. To complete the formulation, boundary conditions are determined to simplify the 2D solution domain as presented in Fig. 1(a). The boundary conditions can summarize as below:

The entrance the domain:

$U_1 = 1,\ U_2 = T^* = 0$

Symmetric lines:

$\partial U_1/\partial y^* = 0,\ \ U_2 = 0,\ \partial T^*/\partial y^* = 0$

The exit of the domain:

$\partial U_1/\partial x^* = 0,\ \ \partial U_2/\partial x^* = 0,\ \partial T^*/\partial x^* = 0$

The surface of tubes:

$U_1 = 0,\ U_2 = 0,\ T^* = 1$

The set of conservation Eqs. (3) to (5) can be generally written in Cartesian coordinates as Eq. (6).

$$\frac{\partial(U_1\phi)}{\partial x^*} + \frac{\partial(U_2\phi)}{\partial y^*} = \frac{\partial}{\partial x^*}\left(\Gamma\frac{\partial\phi}{\partial x^*}\right) + \frac{\partial}{\partial y^*}\left(\Gamma\frac{\partial\phi}{\partial y^*}\right) + S_\phi^* \tag{6}$$

The continuity equation, Eq. (3), without diffusion and source terms, can be used to derive an equation for correcting pressure. The grid generation scheme based on elliptic partial differential equations is used in the present study to generate curvilinear coordinates. Eq. (6) can be transformed from the physical to computational domain on the basis of the following transformation $\xi^* = \xi^*(x^*, y^*), \eta^* = \eta^*(x^*, y^*)$ [15, 16]. The schematic of the computational grid is illustrated in Fig. 1(b).

The final form of the transformed equation can be written as Eq. (7):

$$\frac{\partial}{\partial\xi^*}(\phi G_1^*) + \frac{\partial}{\partial\eta^*}(\phi G_2^*) = \frac{\partial}{\partial\xi^*}\left[\frac{\Gamma}{J}\left(\alpha\frac{\partial\phi}{\partial\xi^*} + \gamma\frac{\partial\phi}{\partial\eta^*}\right)\right] + \frac{\partial}{\partial\eta^*}\left[\frac{\Gamma}{J}\left(\beta\frac{\partial\phi}{\partial\eta^*} + \gamma\frac{\partial\phi}{\partial\xi^*}\right)\right] + J^*\times S_\phi^* \tag{7}$$

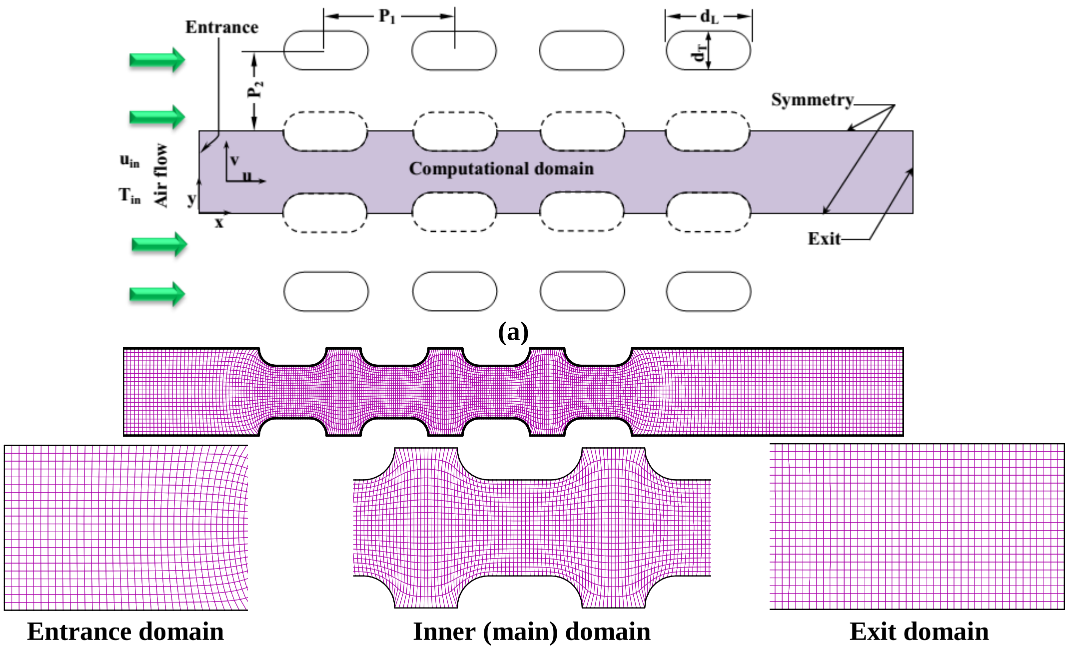

(b)

Fig. 1. In-line flat tube bank (a) tube arrangement and computational domain, and (b) schematic of computational grid systems generated by the body-fitted coordinates.

which are expressed as follows:

$$\left.\begin{aligned}
G_1^* &= U_1\frac{\partial y^*}{\partial\eta} - U_2\frac{\partial x^*}{\partial\eta},\\
G_2^* &= U_2\frac{\partial x^*}{\partial\xi} - U_1\frac{\partial y^*}{\partial\xi},\\
J &= \frac{\partial y^*}{\partial\xi}\frac{\partial x^*}{\partial\eta} - \frac{\partial x^*}{\partial\xi}\frac{\partial y^*}{\partial\eta},\\
\alpha &= \left(\frac{\partial x}{\partial\eta}\right)^2 + \left(\frac{\partial y}{\partial\eta}\right)^2,\\
\beta &= \left(\frac{\partial x}{\partial\xi}\right)^2 + \left(\frac{\partial y}{\partial\xi}\right)^2,\\
\gamma &= \left(\frac{\partial x}{\partial\xi}\frac{\partial x}{\partial\eta}\right) + \left(\frac{\partial y}{\partial\xi}\frac{\partial y}{\partial\eta}\right)
\end{aligned}\right\} \tag{8}$$

This study determines the overall Nusselt number, the Coburn j-factor, the friction factor or the resulting air flow, and the temperature fields, which are expected to represent the total pressure drop for the flat tube bank system.

The overall Nusselt number, (Nu), is defined as follows:

$$\mathrm{Nu} = \frac{h \times D_h}{k} \tag{9}$$

The calculation of the Colburn j-factor is presented through the following non-dimensional parameter:

$$j = \frac{\mathrm{Nu}}{\mathrm{Re}_{D_h} \times \mathrm{Pr}^{1/3}} \tag{10}$$

The friction factor in the expiration is calculated as follows [17]:

$$f = \frac{(p_{\text{in}} - p_{\text{out}})}{2\rho \times (u_{\max})^2 \times N_L} \quad (11)$$

where N_L is the number of transverse rows, which is regarded as
4 in this study.

The mass velocity at minimum flow area can be calculated by Eq. (12) [18]:

$$u_{\max} = u_{\infty} \times \frac{P_T}{(P_T - 1)} \quad (12)$$

2.1. Numerical Methods

The governing equations are solved numerically with the use of FORTRAN 95 (FTN95). The computer code solved the equation of continuity, momentum, and energy, which are discretized by a finite-volume technique. The technique is based on a non-orthogonal coordinate system with Cartesian velocity components and a non-staggered (collocated) grid [19] with the SIMPLE algorithm [20]. The convergence of the steady state is monitored using the determined iterator-to-iterator variations of a field variable that is normalized by its domain. The normalized maximum root-mean-square (RMS) is defined as follows:

$$\text{RMS} = \frac{|\chi_{new} - \chi_{old}|}{(\chi_{max} - \chi_{min})} \quad (13)$$

where χ are U_1, U_2, p^*, and T^*.

The RMS values are checked in every nodal location, and the determined convergences of the upper values of RMS are typically less than 1×10^{-4}.

2.2. Code Validation and Grid Independent Testing

Code validation is an essential aspect of numerical investigation. This section aims to address the code validation issue. The validation with FORTRAN95 (FTN95) code resolved numerous test problems and predictions, which were compared with the code developed from exact solutions, experimental data, or standard problems from previous studies. The numerical model was validated with the publication of certain standard problems. Comparison of the results of this study and Bahaidarah's research [21] are illustrated in Table 1. The results presented in Table 1 include the numerical forecasts of heat transfer by the code, which completely match the numerical forecasts by Bahaidarah [21]. The maximum deviation in the overall Nusselt number is 3.034% or less.

Grid independence test was conducted by modifying the grid numbers with various expansion and contraction factors. The general mesh testing matches the independent solution of the grid. A study was conducted on grid independence test; $P_L = 4.0$ and $P_T = 2.5$ at $Re_{Dh} = 160$ in the domain, and the overall Nusselt number and the friction factor are increased. The study indicated that 601 nodes (along the x-direction) by 21 nodes (along the y-direction) cater to the best results, whereas increases in the number of grids do not affect the result. Table 2 presents the summary of the independent results of the grid. Therefore, to minimize the error and optimum uses of CPU resources, the ideal shape of the grid is 601 × 21.

Table 1
Comparison of overall Nusselt number between the present simulation results and Bahaidarah et al. [21].

	Bahaidarah et al. [21]	Present simulation	Deviation (%)
$Re_{D_h} = 50$			
2nd HEM	9.228	9.508	3.034
3rd HEM	9.229	9.207	0.238
4th HEM	9.229	9.157	0.780
$Re_{D_h} = 200$			
2nd HEM	12.440	12.631	1.535
3rd HEM	12.430	12.532	0.821
4th HEM	12.420	12.424	0.032

% Deviation = $|Nu_{Prov} - Nu_{pres}|/Nu_{prov} \times 100$
HEM: heat exchanger module

3. CALCULATION PROCEDURE FOR ANN MODEL

ANNs are information processing systems that possess certain properties that work effectively with biological neural networks. ANNs are one of the most commonly used and developed models in investigating the relationship between linear or non-linear input-output patterns. The neural network is a mapping between its inputs and outputs based on a number of known sample input-output pairs. Moreover, ANNs facilitate the training and the approximation of the test team. Performance of ANN usage has predictable success. The literature provides numerous detailed ANN types that are related to the approximation function [22,23]. Schematic diagrams for specific artificial intelligence models used in the analysis are shown in Fig. 2. The first input layer feeds data to a hidden intermediate layer. The hidden layer processes the data and transports it to the

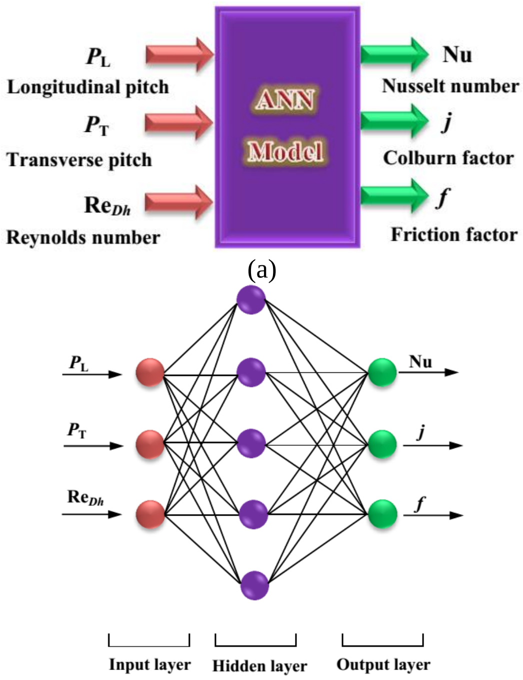

Fig. 2. Typical scheme for system models (a) input and output, and (b) Configuration on a 3-5-3 the neural networks.

Table 2
Results of grid independence test and proportional error analysis with different grid sizes at P_L = 4.0, P_T = 2.5 and Re_{Dh} = 160.

No. of grids in x^*-direction	No. of grids in y^*-direction	Overall Nusselt number	Nu % diff.	Friction factor	f % diff.
401	21	16.1702	-	0.0265	-
501	21	15.8731	1.872	0.0270	1.852
601	21	15.7470	0.801	0.0272	0.735
601	21	15.7227	0.155	0.0273	0.366
601	**21**	**15.7125**	**0.065**	**0.0273**	**0.0**
601	31	15.7117	0.005	0.0274	0.365
601	41	15.7104	0.008	0.0275	0.364

% diff $= \left|\varphi_{(i+1)} - \varphi_i\right| / \varphi_{(i+1)} \times 100$; φ is any parameters.

output layer. Only the tap weights between the hidden layer and the output layer are modified during training. Each hidden layer neuron represents a basis function of the output space with respect to a particular center in the input space. The second layer is the hidden layer which is composed of nonlinear units that are connected directly to all of the nodes in the input layer. It is of high enough dimensions which serves a different purpose from that in a multilayer perceptron. Each hidden unit takes its input from all the nodes at the components of the input layer and the hidden units contain a basis function, which has the parameters center and width. The transformation from the input space to the hidden unit space is nonlinear, whereas the transformation to the hidden unit space to the output space is linear. The neural networks were determined with the use of MATLAB program, and all of the tests were implemented in a computer. Activating the error function in this study is a function of the logistic sigmoid and the standard total of the squared error function.

The data that was numerically evaluated in this study were normalized to obtain the values by using the following Eq. (14):

$$\left(\frac{\text{Actual} - \text{Minimum}}{\text{Maximum} - \text{Minimum}}\right)_{\text{data}} \times (\text{High data} - \text{Low data}) + \text{Low data} \qquad (14)$$

where the maximum and minimum are the maximum and minimum data values, respectively, such that, the low is the minimum normalized data value = 0.1, and the high is the maximum normalized data value = 0.9 [20]. In general, the proposed correlations formula can be assessed statistically by measuring the coefficient of determination, R^2, as pointed out by Kvalseth [25]. The R^2–value is mostly computed with the use of data points. The R^2–value is the standard of the appropriateness of the regression model designed for the fitted test data [26]. R^2 = 1 refers to the perfect correlation when all of the residuals (the difference between the estimated and the actual data values at each test point) are equal to zero.

The relative error (Er) for variable (ψ), and the mean relative error (MEr) between the empirical and predicted data is estimated by Eq. (15) [27]:

$$\left.\begin{aligned} \text{Er}(\%) &= \frac{|\psi^N - \psi^P|}{\psi^N} \times 100 \\ \text{MEr}(\%) &= \frac{1}{n}\sum_{i=1}^{n} \text{Er}(\%)_i \end{aligned}\right\} \qquad (15)$$

The root mean square error (RMSE) can be evaluated by Eq. (16) [28]:

$$\text{RMSE} = \left[\frac{1}{n}\sum_{i=1}^{n}(\psi^N - \psi^P)_i^2\right]^{1/2} \qquad (16)$$

The correlation coefficient (R^2) is defined by [29]:

$$R^2 = 1 - \frac{\sum_{i=1}^{n}(\psi^N - \psi^P)_i^2}{\sum_{i=1}^{n}(\psi^N)_i^2} \qquad (17)$$

where (N) is the numerical data, (P) is the predicted result, and (n) is the number of numerical data.

4. RESULTS AND DISCUSSION

Numerical evaluations were conducted to verify the results of the ANN model. Sixty numerical simulation data were utilized to produce the ANN model. To improve the proposed model, data from 46 cases (approximately 76.67%) were used for training, and the remaining 14 cases were used for the testing performance (approximately 23.33%) to evaluate the ANN model. The original data (CFD) that were employed to produce the ANN model are listed in Table 3.

Results of the developed ANN model with the training data are shown in Fig. 3. The figure shows the overall Nusselt number, Colburn j-factor, and friction factor. An excellent agreement exists between the output data from the ANN model and the data obtained from the simulations; the maximum relative error are approximately ±3.84%, ±5.87%, and ±13.87%, and the mean relative error are approximately 1.43%, 2.43%, and 5.57%, for the Nusselt number, Colburn j-factor, and friction factors, respectively. For the overall Nusselt number, the best agreement between the ANN predictions and the CFD simulation results (R^2=99.916%) are provided in Fig. 3(a). The j-factor predictions of ANN that were in excellent agreement with the numerical simulation results (R^2 = 99.947%) are depicted in Fig. 3(b). The predictions of the ANN for the friction factor that were in best agreement with the CFD simulation results (R^2 = 99.914%) are indicated in Fig. 3(c), which is a powerful indication of excellent data fitting. Performance through the ANN models is assessed on the basis of the statistical evaluation

Table 3
The original (CFD) values using in the training and testing of the ANN model.

Run no.	P_L	P_T	Re_{Dh}	Nu	j	f	Run no.	P_L	P_T	Re_{Dh}	Nu	j	f
1,TS	3	1.5	10	7.236	0.811	0.935	31,TS	4	3.5	10	5.885	0.659	0.293
2,TS	3	1.5	40	10.339	0.290	0.246	32,TR	4	3.5	40	8.576	0.240	0.074
3,TR	3	1.5	80	12.311	0.172	0.117	33,TR	4	3.5	80	10.324	0.145	0.036
4,TR	3	1.5	160	14.344	0.100	0.058	34,TR	4	3.5	160	14.173	0.099	0.019
5,TR	3	1.5	320	18.127	0.063	0.038	35,TR	4	3.5	320	15.874	0.056	0.013
6,TS	3	2.5	10	6.512	0.730	0.401	36,TS	4	4.5	10	5.629	0.631	0.276
7,TR	3	2.5	40	9.305	0.261	0.099	37,TR	4	4.5	40	8.216	0.230	0.069
8,TR	3	2.5	80	11.080	0.155	0.047	38,TR	4	4.5	80	9.890	0.139	0.034
9,TR	3	2.5	160	12.910	0.090	0.023	39,TR	4	4.5	160	13.577	0.095	0.018
10,TR	3	2.5	320	16.314	0.057	0.015	40,TR	4	4.5	320	15.207	0.053	0.012
11,TS	3	3.5	10	5.868	0.658	0.300	41,TS	6	1.5	10	7.238	0.811	0.975
12,TR	3	3.5	40	8.384	0.235	0.074	42,TR	6	1.5	40	10.645	0.298	0.154
13,TR	3	3.5	80	9.983	0.140	0.035	43,TR	6	1.5	80	12.781	0.179	0.139
14,TR	3	3.5	160	11.632	0.081	0.017	44,TR	6	1.5	160	17.769	0.124	0.076
15,TR	3	3.5	320	14.699	0.051	0.012	45,TR	6	1.5	320	19.877	0.070	0.052
16,TS	3	4.5	10	5.615	0.629	0.263	46,TS	6	2.5	10	6.586	0.738	0.437
17,TR	3	4.5	40	8.023	0.225	0.065	47,TR	6	2.5	40	9.687	0.271	0.115
18,TR	3	4.5	80	9.554	0.134	0.031	48,TR	6	2.5	80	11.631	0.163	0.058
19,TR	3	4.5	160	11.131	0.078	0.015	49,TR	6	2.5	160	16.169	0.113	0.032
20,TR	3	4.5	320	14.067	0.049	0.010	50,TR	6	2.5	320	18.088	0.063	0.022
21,TS	4	1.5	10	7.238	0.811	0.955	51,TS	6	3.5	10	5.943	0.666	0.322
22,TS	4	1.5	40	10.564	0.296	0.261	52,TR	6	3.5	40	8.742	0.245	0.085
23,TR	4	1.5	80	12.717	0.178	0.127	53,TR	6	3.5	80	10.495	0.147	0.043
24,TR	4	1.5	160	17.458	0.122	0.067	54,TR	6	3.5	160	14.591	0.102	0.023
25,TR	4	1.5	320	19.554	0.068	0.047	55,TR	6	3.5	320	16.322	0.057	0.016
26,TS	4	2.5	10	6.514	0.730	0.420	56,TS	6	4.5	10	5.700	0.639	0.277
27,TR	4	2.5	40	9.508	0.266	0.106	57,TR	6	4.5	40	8.383	0.235	0.073
28,TR	4	2.5	80	11.445	0.160	0.051	58,TR	6	4.5	80	10.065	0.141	0.037
29,TR	4	2.5	160	15.713	0.110	0.027	59,TR	6	4.5	160	13.993	0.098	0.020
30,TR	4	2.5	320	17.599	0.062	0.019	60,TR	6	4.5	320	15.653	0.055	0.014

TR, TS are the training and testing data selected for training and testing the ANN model, respectively.

functions mentioned in Eqs. (15)-(17), as commonly employed [11,23,29].

The predicted results of the testing deviation values for overall Nusselt number were MEr = 0.39%, RMSE =3.28×10^{-2}, whereas in predicting j-factor the values were MEr = 1.54%, RMSE = 8.88×10^{-3}, and for friction factor, they were MEr = 4.50%, RMSE = 2.11×10^{-2}. The comparisons of testing data sets for the predicted value results of the overall Nusselt number, j-factor, and friction factor of the developed ANN and the original data (CFD simulation) are plotted in Fig. 4, where the solid line refers the ideal fit (predicted equal original data). The excellent agreement of the figures among the ANN predicted results and the original values with the correlation coefficient higher than R^2 = 99.505% are notable. Furthermore, lower MRE and MSE values of the test data sets, as well as the difference between the values of acceptable deviation to teas and train data sets, refers to the verification of the ANN models. In addition, the overall Nusselt number, j-factor, and friction factor for the testing data predicted by ANN and actual (CFD) with different geometry and flow parameters are tabulated in Table 4. The maximum relative error was determined at approximately ±1.068%, ±4.369%, and ±6.592%, for overall Nusselt number, j-factor, and friction factor, respectively.

Utilizing the Eq. (15) on the original CFD value to produce the relative error results of the ANN model for the training and testing data is shown in Fig. 5. Fig. 5(a) clearly illustrates the maximum relative errors ($Er_{\max}$) for overall Nusselt number are approximately ±1.07% for testing and ±3.85% for training, with the mean relative error (*ME*r) at 0.39% and 1.43%, respectively. The relative error of j-factor is presented in Fig. 5(b). The $Er_{\max}$ are approximately ±4.39% for testing and ±5.87% for training, with the *ME*r at 1.55% and 2.43%, respectively. The f factor's ANN prediction against the CFD values are presented in Fig. 5(c). The ANN yields $Er_{\max}$ at approxim-

Table 4
Comparison the overall Nusselt number, *j*-factor and friction factor of numerical and ANN model for testing data.

Run no.	1	2	6	11	16	21	22	26	31	41	46	51	56
							Overall Nusselt number						
CFD	7.236	10.339	6.512	5.868	5.615	7.238	10.564	6.514	5.875	5.629	7.238	6.586	5.943
ANN	7.243	10.339	6.582	5.837	5.626	7.174	10.564	6.527	5.832	5.651	7.238	6.618	5.909
%Er	0.096	0.001	1.068	0.519	0.190	0.884	0.001	0.205	0.734	0.403	0.006	0.481	0.580
%MEr							0.390						
							Colburn j-factor						
CFD	0.811	0.290	0.730	0.658	0.629	0.811	0.296	0.730	0.659	0.631	0.811	0.738	0.666
ANN	0.815	0.278	0.736	0.663	0.637	0.807	0.309	0.726	0.650	0.619	0.799	0.747	0.679
%Er	0.527	4.159	0.787	0.862	1.248	0.579	4.396	0.570	1.353	1.836	1.470	1.152	1.884
%MEr							1.535						
							Friction factor						
CFD	0.935	0.246	0.401	0.300	0.263	0.955	0.261	0.420	0.293	0.276	0.975	0.437	0.322
ANN	0.987	0.230	0.411	0.320	0.278	0.958	0.246	0.393	0.297	0.263	0.965	0.410	0.305
%Er	5.664	6.283	2.489	6.469	5.640	0.326	5.722	6.592	1.384	4.805	1.017	6.169	5.142
%MEr							4.500						

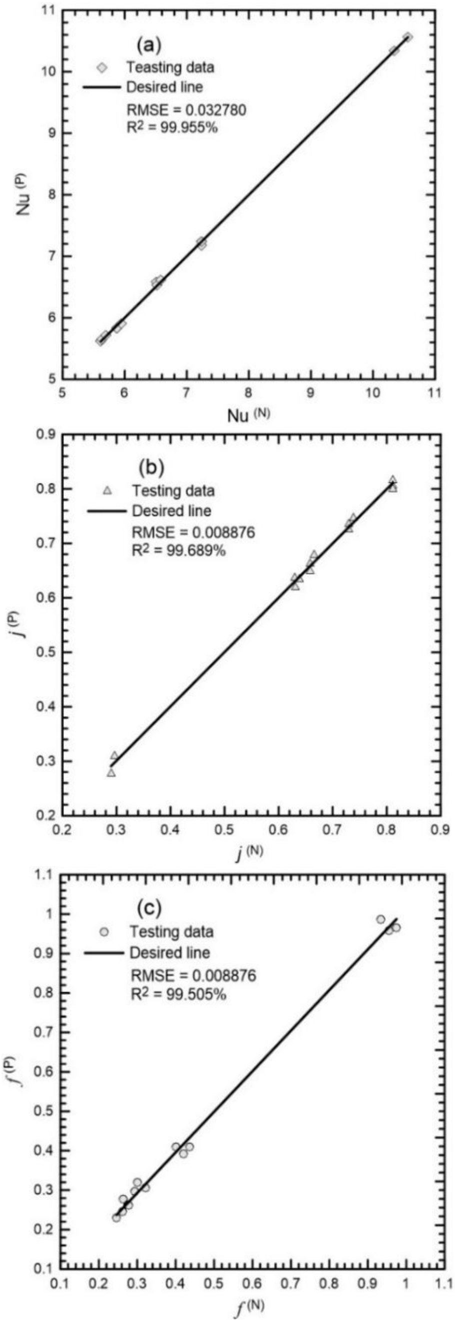

Fig. 4. The testing results evaluated using ANN for (a) overall Nusselt number, (b) ***j***-factor and (c) ***f*** factor.

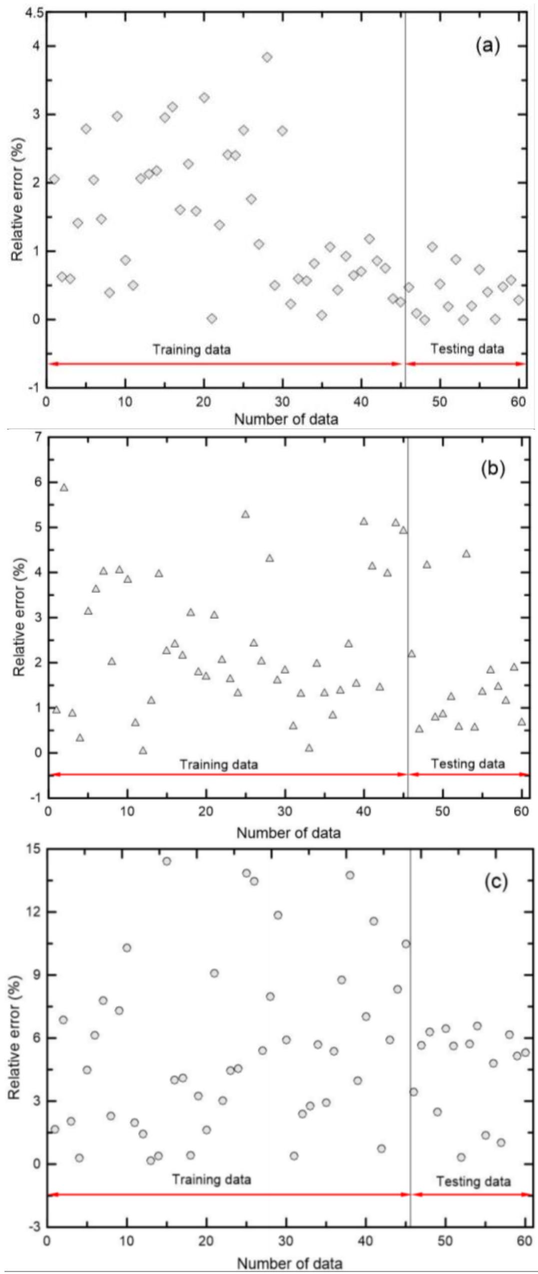

Fig. 5. The relative error for training and testing data using (a) overall Nusselt number (b) *j*-factor and (c) *f* factor.

ately ±6.59% for testing and ±13.87% for training, with the *ME*r at 4.50% and 5.57%, respectively.

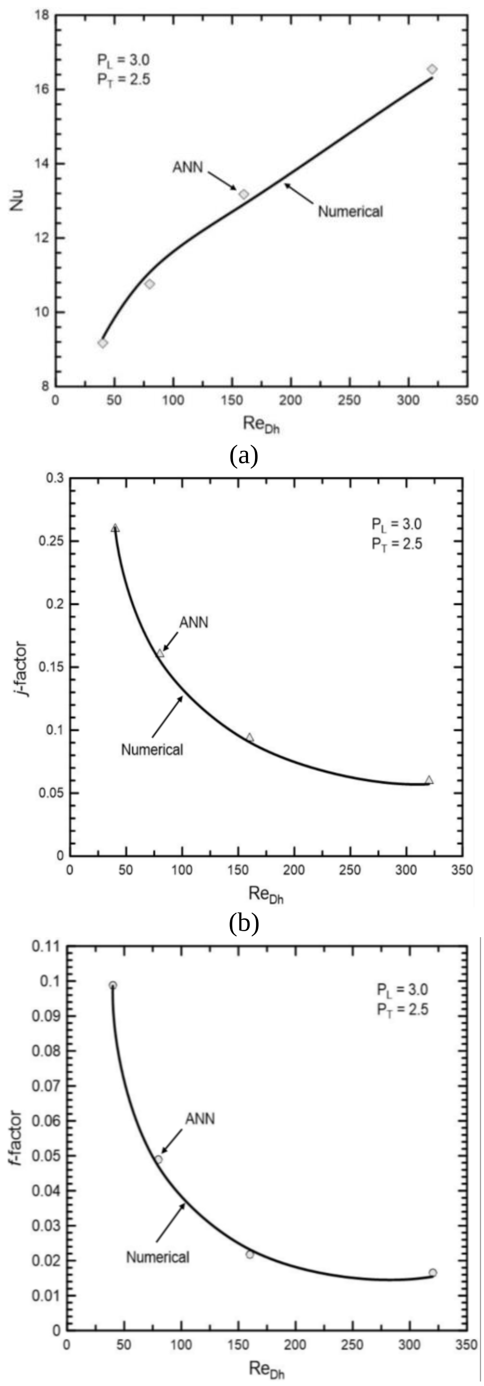

Fig. 6. Comparison of numerical with ANN results against Reynolds number of the training data for (a) overall Nusselt numbers, (b) *j*-factor and (c) *f* factor.

In general, a small relative error was found in the testing data for overall Nusselt number, *j*-factor, and friction factor. The determined ANN predictions were close to the CFD data with minimal deviations for each point of overall Nusselt number. These results indicate that the ANN model is appropriate in predicting the heat transfer coefficient. The numerically calculated data compared with the predicted ANN results for the training data when P_L = 3.0 and P_T = 2.5 relative to Reynolds number are presented in Fig. 6. The used base value (CFD) are shown in Table 3 with numbers 7 to 10, as well as predicted ANN data for overall Nusselt number, *j*-factor, and friction factor. As expected, *Nu* increases with the rise of the Reynolds number as shown in Fig. 6(a). In contrast, *j*- and friction factors decrease with increasing Reynolds number, as demonstrated in Fig. 6(b) and (c). The maximum relative error is found at approximately ±2.79%, ±4.03%, and ±7.78% for overall Nusselt number, *j*-factor, and friction factor, respectively. These trends are extremely similar to the existing CFD results, such that, the initial conditions provided in the ANN model can predict the output variable without implementing any simulation run.

5. CONCLUSIONS

The developed ANN model is applied to estimate the thermal-hydraulic characteristics of in-line flat tubes bank. For all heat transfer and flow parameters, the MEr of the ANN approach range from 1.43% to 5.57% for the training data and from 0.39% to 4.5% for the testing data. The RMSE ranged from 3.67×10^{-3} to 0.219 for the training data and from 8.88×10^{-3} to 3.27×10^{-2} for the testing data. The correlation coefficient for all heat and flow parameters are extremely close to match the lowest value, R^2 = 99.505%. Predicting the thermal-fluids characteristics using ANN approach resulted in a good agreement with the simulation data. Thus, this method is proposed as it offers fast, reliable, and accurate results, as well as initial estimates for an engineer to address complex heat transfer and fluid flow problems.

ACKNOWLEDGMENTS

The authors would like to gratefully acknowledge the Tikrit University and Universiti Malaysia Pahang for the financial support under project no. RDU120103.

REFERENCES

[1] Žukauskas A. Heat transfer from tubes in crossflow. *Advanced Heat Transfer* 1972; **8**: 93–158.

[2] Benarji N, Balaji C, Venkateshan SP. Unsteady fluid flow and heat transfer over a bank of flat tubes. *Heat Mass Transfer* 2007; **44**(4): 445–461.

[3] Kaptan Y, Buyruk E, Ecder A. Numerical investigation of fouling on cross-flow heat exchanger tubes with conjugated heat transfer approach. *International Communication Heat and Mass Transfer* 2008; **35**(9): 1153–1158.

[4] Incropera FP, Dewitt DP, Bergman TL, Lavine AS. Fundamentals of heat and mass transfer. 7th ed. John Wiley & Sons, Inc: USA; 2011.

[5] Min JC, Webb RL. Numerical analyses of effects of tube shape on performance of a finned tube heat exchanger. *Journal Enhanced Heat Transfer* 2004; **11**: 63–76.

[6] Webb RL, Kim N-H. Principle of enhanced heat transfer. 2nd ed. Taylor & Francis: New York; 2005.

[7] Tahseen TA, Ishak M, Rahman MM. An overview on thermal and fluid flow characteristics in a plain plate finned and unfinned-tube banks heat exchanger. *Renewable & Sustainable Energy Reviews* 2015; **43**: 363–380.

[8] Atayılmaz ŞÖ, Demir H, Ağra Ö, Application of artificial neural networks for prediction of natural convection from a heated horizontal cylinder. *International Communication Heat and Mass Transfer* 2010; **37**(1): 68–73.
[9] Ermis K, Erek A, Dincer I, Heat Transfer analysis of phase change process in a finned-tube thermal energy storage system using artificial neural network. *International Journal of Heat and Mass Transfer* 2007; **50**(15–16): 3163–3175.
[10] Fadare DA, Fatona AS. Artificial neural network modeling of heat transfer in a staggered cross-flow tube-type heat exchanger. *Pacific Journal of Science and Technology* 2008; **9**(2): 317–323.
[11] Islamoglu Y, Kurt A. Heat transfer analysis using ANNs with experimental data for air flowing in corrugated channels. *International Journal of Heat Mass and Transfer* 2004; **47**(6–7): 361–365.
[12] Beigzadeh R, Rahimi M. Prediction of heat transfer and flow characteristics in helically coiled tubes using artificial neural networks. *International Communication Heat and Mass Transfer* 2012; **39**(8): 1279–1285.
[13] Tahseen TA, Ishak M, Rahman MM. Heat transfer and pressure drop prediction in an in-line flat tube bundle by radial basis function network. International *Journal of Automotive & Mechanical Engineering* 2015; **10**: 2003-2015.
[14] Bejan A. Convection heat transfer, 2nd ed. USA: John Wiley & Sons Inc.; 2004.
[15] Tannehill JC, Anderson DA, Pletcher RH. Computational fluid mechanics and heat transfer. Second ed. USA: Taylor & Francis; 1997.
[16] Thompson JR, Warsi ZUA, Martin CW. Numerical grid generation, foundations and applications. USA: North-Holland; 1997.
[17] El-Shaboury AMF, Ormiston SJ. Analysis of laminar forced convection of air crossflow in in-line tube banks with nonsquare arrangements. *Numerical Heat Transfer, Part A: Applications* 2005; **48**(2): 99–126.
[18] Holman JP. Heat Transfer, 10th ed., USA: McGraw-Hill Companies, Inc.; 2010.
[19] Ferziger JH, Perić M. Computational methods for fluid dynamics. 3rd ed. USA: Springer-Verlag Berlin Heidelberg; 1999.
[20] Versteeg HK, Malalasekera W. An introduction to computational fluid dynamics the finite volume method. 2nd ed. England: Pearson Education India; 2007.
[21] Bahaidarah HMS, Anand NK, Chen HC. A numerical study of fluid flow and heat transfer over a bank of flat tubes. *Numerical Heat Transfer, Part A: Applications* 2005; **48**(4): 359–385.
[22] Tahseen TA, Ishak M, Rahman MM. Performance predictions of laminar heat transfer and pressure drop in an in-line flat tube bundle using an adaptive Neuro-Fuzzy Inference System (ANFIS) model. *International Communications in Heat and Mass Transfer* 2014; **50**: 85–97.
[23] Kalogirou SA. Applications of artificial neural-networks for energy systems. *Applied Energy* 2000; **67**(1): 17–35.
[24] Nasr GE, Badr EA, Joun C. Backpropagation neural networks for modeling gasoline consumption. *Energy Conversion and Management* 2003; **44**(6): 893–905.
[25] Kvalseth TO. Cautionary note about R^2. *American Statistician* 1985; **139**: 279–85.
[26] Hayati M, Rezaei A, Seifi M. Prediction of the heat transfer rate of a single layer wire-on-tube type heat exchanger using ANFIS. International Journal of *Refrigeration* 2009; **32**(8): 1914–1917.
[27] Akdag U, Komur MA, Ozguc AF. Estimation of heat transfer in oscillating annular flow using artifical neural networks. *Advances in Engineering Software* 2009; **40**(9): 864–870.
[28] Junqi D, Jiangping C, Zhijiu C, Yimin Z, Wenfeng Z, Heat transfer and pressure drop correlations for the wavy fin and flat tube heat exchangers. *Applied Thermal Engineering* 2007; **27**(11): 2066–2073.
[29] Koronaki I, Rogdakis E, Kakatsiou T. Thermodynamic analysis of an open cycle solid desiccant cooling system using artificial neural network. *Energy Conversion and Management* 2012; **60**: 152–160.